Benha Journal of Applied Sciences (BJAS) **print: ISSN 2356–9751**
Vol. (10) Issue (7) (2025), (107- 116) **online: ISSN 2356–976x**

https://bjas.journals.ekb.eg/
engineering sciences

Numerical analysis of cold-formed built-up closed-section subjected to axial load

Kareem M. Abdelkareem, Hanan H. Eltobgy, Mohamed M. El-Saadawy, and Khaled A.Gharib
Civil Engineering Dept., Faculty of Engineering, Benha University, Egypt.
E-mail: km457395@gmail.com

Abstract

Cold-formed steel (CFS) is frequently utilized in construction owing to its lightweight, ease of production, straightness, and durability. These properties make CFS an ideal choice for various structural applications, including framing, roofing, cladding systems, straightforward quality control, and cost-efficient transportation compared to traditional materials. It also allows for the flexible design of cross-sectional profiles and is fully recyclable. This study presents a numerical analysis of built-up columns fabricated from cold-formed steel. Ten built-up steel columns were analyzed, differing in thickness (1 mm and 2 mm) and varied in length (1200 mm, 2000 mm , 3000mm and 4500mm), under pin-ended boundary conditions. The cross-sections are manufactured by composing two identical zee sections with stiffener in web and channels using self-tapping screws. The specimens were modelled using ABAQUS software, incorporating material properties and geometric imperfections into the finite element (FE) models. The results of the numerical simulations closely matched previous experimental findings for built-up closed columns subjected to compressive loads, thus validating the FE model. The study revealed that axially loaded columns with varying slenderness ratios exhibited different failure modes, including local buckling, local-flexural buckling, and flexural-distortional buckling.

Keywords*:* Cold-formed steel, Z section, built-up section, Buckling, Axial Load, Finite element.

1. Introduction

CFS is gaining popularity in construction due to its low cost, lightweight, high strength-to-weight ratio, and ease of manufacturing. The built-up CFS composed of double Zee-stiffener sections with channel column is an example of a cold-formed steel component used in trusses and residential and commercial construction. The study identifies the ideal screw spacing by analyzing several configurations of double Zee-stiffener sections with channel designs and differing screw spacings, leading to enhanced strength properties. The Abaqus software will be utilized to examine the impact of screw quantity on the structural performance of assemblies comprising two Zee-stiffener sections with a channel CFS column. First of all, the techniques and the methods available in the literature will be illustrated. Turabian et al. [1] tested the built-up zee-sections column subjected to bi-axial bending and axial compression. According to Torabian et al., experimental experiments demonstrated that the AISI S100 (2012) [2]-recommended simple linear interaction approach yields conservative forecasts for column member strength. A numerical and experimental study of double-Z built-up members under uniaxially compressive loads was conducted by I. Georgieva et al. [3]. According to Georgieva et al. [3], medium and long columns experienced flexural-torsional buckling, whereas short columns had distortional failure. Gunalan et al. [4] investigated the local buckling behavior of cold-formed steel unlipped and lipped channel sections at higher temperatures experimentally and numerically [5]. They also examined the combined flexural and torsional buckling in cold-formed steel-lipped channels exposed to axial compression at elevated temperatures.

A study by I. Georgieva et al. [6] evaluated a double-Z built-up member fastened with bolts. This member underwent bending as well as compression. It should be noted that all of these tests have only taken into account built-up portions made up of two comparable components in which both components buckle at the same time. Ozturk et al. [7] investigated the structural behavior of eccentrically loaded beam–column CFS lipped and sigma channel profiles by an experimental and analytical study. Compared to those with lipped channel sections, it was demonstrated that short beam-columns with sigma sections frequently have up to 42% greater strength. In an experimental investigation, Qiu-Yun Li et al. [8] subjected open built-up sections to eccentric compressive load while they were fastened with self-drilling screws. The cross-section consisted of twin channels CFS with longitudinal stiffeners, and the specimen lengths reached up to 1500 mm. The axial load-moment interaction calculations were shown to often underestimate the strength of the cold-formed steel built-up open-section columns. A thorough analysis of the literature study shows that most of the studies were concerned only with built-up cross-sections composed of channel, I section, angles, or zed sections. Conversely, CFS is composed of double Zee-stiffener sections with channel columns subjected to compressive load

approximately were not investigated. As a result, much more work needs to be done. The structural performance of CFS built-up columns made of Zee-stiffener sections with channel under axial compression will be investigated numerically in this research. Additionally, built-up CFS columns subjected to compressive loads will have their ultimate load capacity and failure modes indicated. A parametric study was conducted to examine the effects of screw spacing, member length, and section thickness based on the Finite Element (FE) results of 20 verified models. The dimensions of the CFS built-up sections under consideration are displayed in table 2.

2. FE Model investigation

2.1 General description

A numerical model that incorporates the elastic and plastic responses of a cold-formed steel battened column was developed using ABAQUS [9] and a non-linear finite element. Creating a reliable simulation of the behavior of battened columns composed of built-up cold-formed steel (BCFS) is the goal of this model. The geometry of the model and the material properties are described in the analysis section that follows.

Two stages of assessment are required when employing finite element methods for buckling analysis. Finding the analysis of the columns' buckling modes of forms by Eigenvalue is the first step. The (*BUCKLE) command from the ABAQUS library is used in the elastic linear analysis, with the applied load occurring at a specified step. Several buckling modes are assessed in this analysis, and the most relevant mode found by the Eigenvalue analysis is selected. In the second step, a nonlinear load-displacement analysis is conducted, taking into account the material's nonlinearity and initial defects. The ultimate capacity, stresses, axial shortenings, failure modes of form, and lateral displacement of the columns are all determined by this comprehensive analysis.

2.2 Finite element mesh and materials modelling

Using the S4R shell element from the ABAQUS library, each portion of the cold-formed section was simulated using end-loading plates, batten plates, and CFS channels in the ABAQUS finite element software.

In the ABAQUS program, each node in this shell element has six degrees of freedom and is utilized in a variety of usages. A revised mesh of three-dimensional four-node bilinear rigid quadrilateral shell elements (R3D4) from the ABAQUS element collection was used to model the bottom and upper-end plates.

To determine the ideal mesh that guarantees enough accuracy while reducing computing time for modelling cold-formed steel built-up section Zee-stiffener sections with channel columns, convergence techniques research was carried out. A finer mesh was used at the corners, as shown in Fig. 1, and a small mesh size of 5 × 5 mm (length × width) produced adequate precision in modelling the built-up section columns. As shown in Fig. 1, a reference point was positioned perpendicular to the plane of each end plate and pointed in the direction of the plate's center.

The effective length of each specimen between the two articulated supports is indicated by the reference points. The load was assigned to the RP of the upper-end plate, and the boundary conditions were applied to the RPs. During the loading method, a "Tie" constraint in ABAQUS is used to represent the top loading plate for the cold-formed steel C-channels. Throughout the loading process, this instruction guarantees that the associated parts' rotations and displacements remain consistent. In ABAQUS [9], three-dimensional shell meshes can be automatically connected by using the tie constraint. Bilinear or idealized finite element analysis is used to simplify and approximate the stress-strain relationship. The cross-section is subject to this approximation. A multilinear stress-strain curve can be used with ABAQUS thanks to its flexible features, which show how well it can handle different material behaviors. The characteristics of carbon steel were investigated in this parametric study. The characteristics of carbon steel were investigated in this parametric study. Von Misses isotropic hardening is used to model steel, which has an ultimate strength (Fu) of 5300 MPa and a minimum yield (Fy) of 360 MPa. The shear modulus that we used was 81500 MPA. The bilinear elastic-plastic stress-strain curve is used to imitate steel. Young's modulus of Eo = 216 GPa and Poisson's ratio of 0.3 were employed in the linear elastic portion of the curve. The model's nonlinear analysis grows isotopically as plastic hardens from an isotropic yield surface based on the Von Mises criterion.

2.3 loads and Boundary conditions fastener and contact modelling

The behavior of pin-ended built-up columns with cold-formed sections was simulated using a finite element analysis using the ABAQUS software.

To reproduce the pin-ended supports, Figure 1 shows how to apply displacements and rotations (boundary conditions) at the upper and lower reference points (RPs).

Figure 2 depicts the CONN3D2 element, which is a three-dimensional beam connector with two nodes and six degrees of freedom per node used to represent the self-drilling screws [10,11].

The analysis process was similar to that of similar previous investigations [12]. The columns' higher points were stopped from rotating on the Z-axis and from translating in the X and directions. As shown in Figure 2, the column end conditions were restricted against rotation in the Z direction and translations in the X, Y, and Z axes.

The force at the end plate RP was subjected to a load.

A modified version of the RIKS approach from the ABAQUS [9] library was used to apply the load gradually. The required loading and boundary conditions are used in this column investigation under axial compressive force (pu).

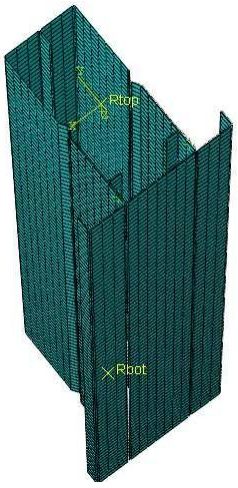

Load positions

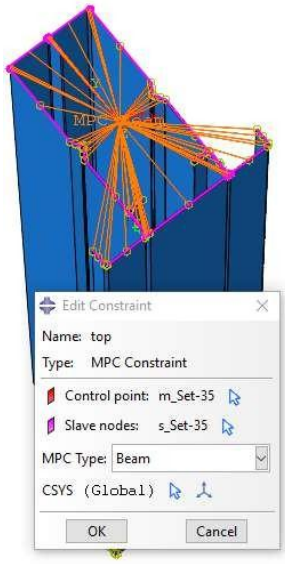

MPC

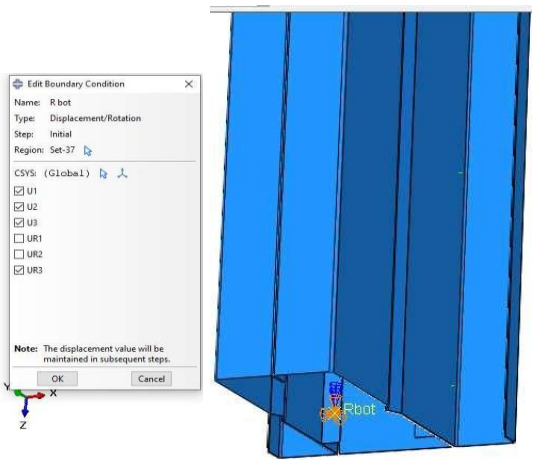

a. Boundary conditions

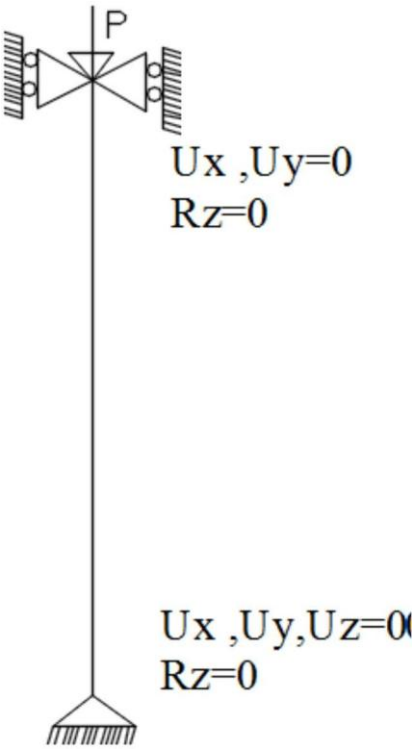

b. Finite elements mesh, load application, and Boundary condition

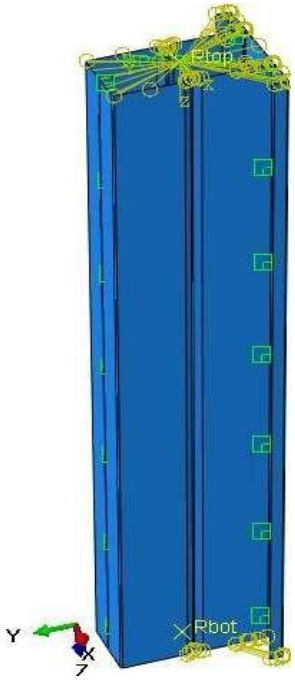

Fig.(1) Numerical modeling a) Finite elements mesh, load application, and Boundary condition b) arrangement of bolts**.**

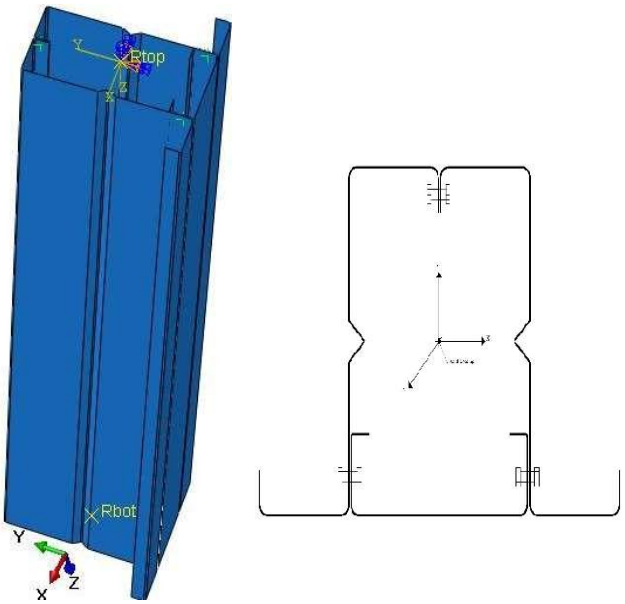

Fig.(2) Loading positions at column upper loaded end and support position at column lower support end for column subjected to axial loads.

2.4 Initial geometric imperfections

The finite elements under analysis consider both local buckling and overall buckling failure modes' measured magnitudes.

It is possible to determine the buckling modes and outline the general flaws in the column by doing eigenvalue evaluations. According to the literature review, the average overall defects for the studied specimens were 1/1000 of the specimen's total length [20]. In battened columns made from assembled cold-formed steel parts, imperfections were replicated. The eigenvalue analysis of all buckling modes predicted by ABAQUS [9] is standardized to 1.0. Additionally, Figure 3 shows the measurement of the overall geometric and initial local defects in the buckling modes.

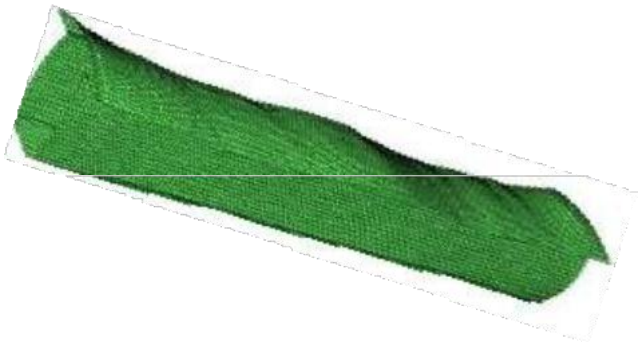

Fig.(3) Initial geometric imperfection modes

3. Verification of the developed Finite Element Model

The author utilizes prior experimental and computational work by F. Meza on cold-formed steel built-up stub columns exposed to compressive loads to verify the finite element model results. Table 1 presents the specimens' nominal dimensions and material attributes previously tested.

Figure 4. a, b&c. shows the analysis of the correlations between the test results, the deformed shape, load vs axial shortening, and load versus lateral displacement. Table 1 shows that the values of the current finite element model and the experimental ultimate loads have an acceptable connection.

A substantial connection is shown when the Finite Element Analysis (FEA) findings are compared to the experimental data in the four dimensions—peak strength, failure mode, axial shortening, and the load against displacement relationship. Consequently, the proposed parametric studies fit the finite element model well.

Table (1) Dimensions, material properties and results of previous experimental test F. Meza et al. [10] and verified FE model by author.

Specimen	Section	Height (mm)	h_w (mm)	b_f (mm)	t (mm)	E (GPa)	σ0.2% (MPa)	Results Pu (kN) FEM&Exp. Test [Meza et al.] [10]	Results Pu (kN) FEM By author	Error (%)
LC2-4	T15414	1800	154	54	1.4	198	280	163.025	166.277	
	T7912		79	36	1.4	203	281			
Failure mode								LB	LB	
Pu FEM/Pu Exp. [10]								1.02		1.96

LB = local buckling

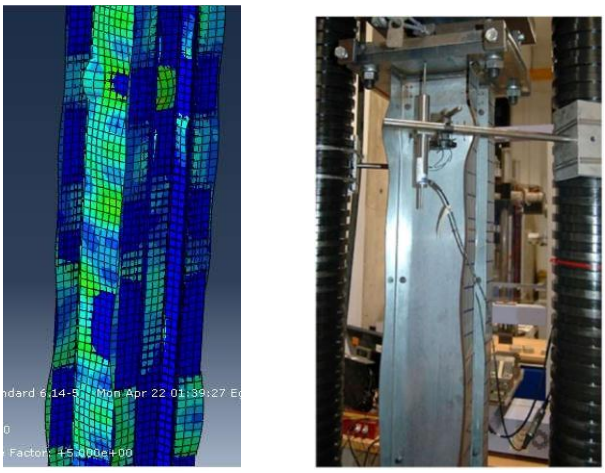

Fig.(4. a) Verification of pervious experimental test result by F. Meza et al. [10] versus FEM Author

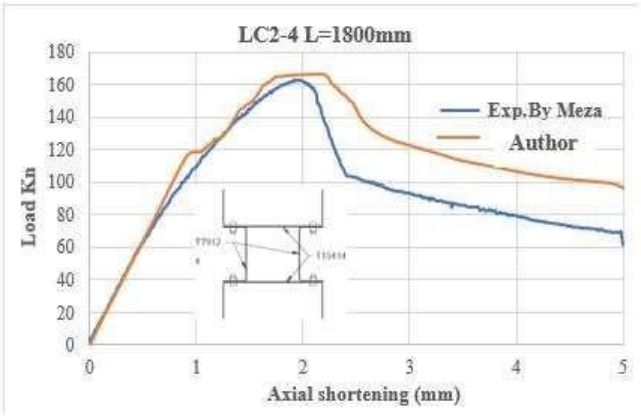

Fig.(4. b) Load -Axial shortening relationships

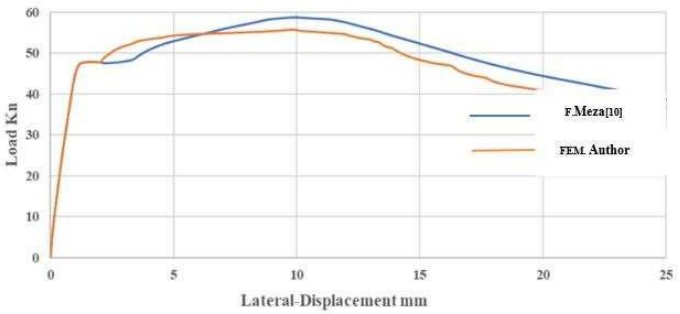

Fig.(4. c) Lateral displacement-load relationships

3.1 Parametric study

The parametric analysis evaluated columns with differing thicknesses of the built-up cross-section, shown in Figure 5. A total of 10 columns were evaluated, with dimensions illustrated in Figure 6 and defined in Table 2. According to Figure 6, the column lengths were 1200 mm, 2000 mm, 3000 mm, and 4500 mm. Each column subjected to axial compressive loading as shown in Figure 2.

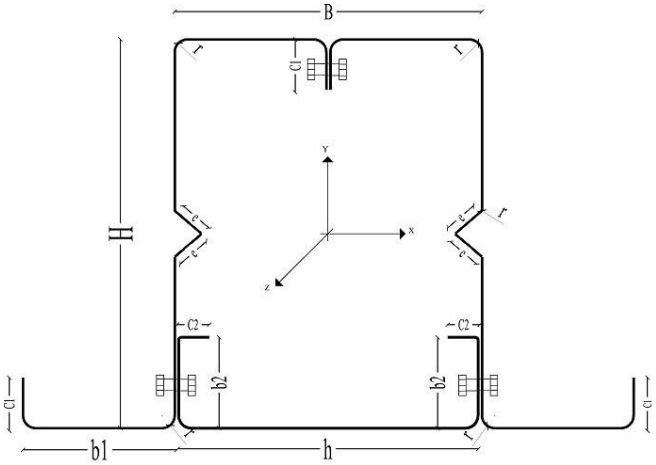

Fig.(5) The cross-sectional dimensions for the parametric study.

The dimensions of the Zee section, which include web depth (H), flange width (b1), and lip depth (c1), as well as the dimensions of the channel section, including web depth (h), flange width (b2), and inner corner radius of the built-up section (r), are provided in Table 2. This table also includes the nominal dimensions of the tested specimens. Additionally, the overall depth (B) of the column cross-section and the thicknesses of the Zee and channel sections (tz and tc, respectively) are shown in Table 2. The Zee section dimensions, including web depth (H), flange width (b1), and

lip depth (c1), in addition to the channel section dimensions, including web depth (h), flange width (b2), and inner corner radius of the built-up section (r), are listed in Table 2 together with the nominal dimensions of the tested specimens. The overall depth (B) of the column cross-section and the thickness of the Zee & the channel (tz & tc), respectively, are shown in Table 2.M6 self-drilling sheet metal screws and the arrangements shown in figure 6 were used to assemble the built-up column cross-section components. Figure 7 illustrates the designations for specimen labels.

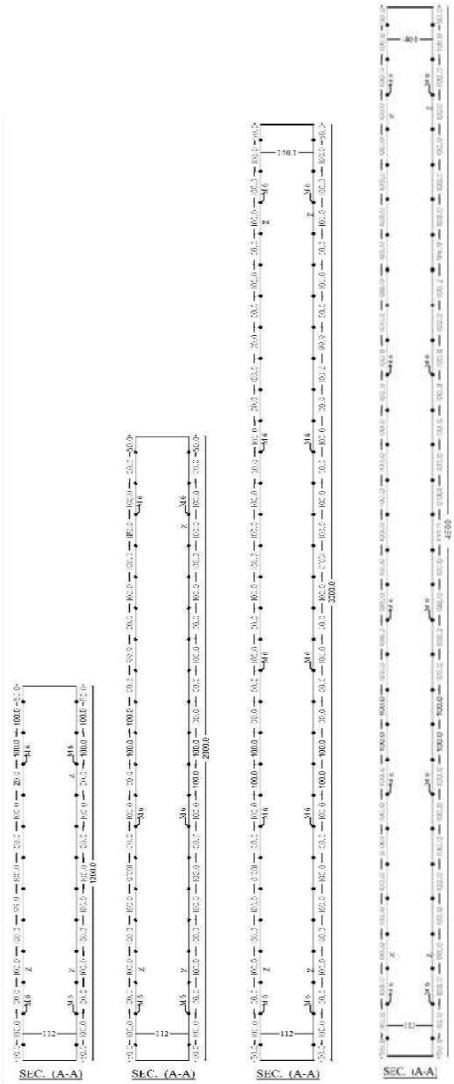

a. Columns length (1200,2500,3000,4500) with spacing 100mm between screws

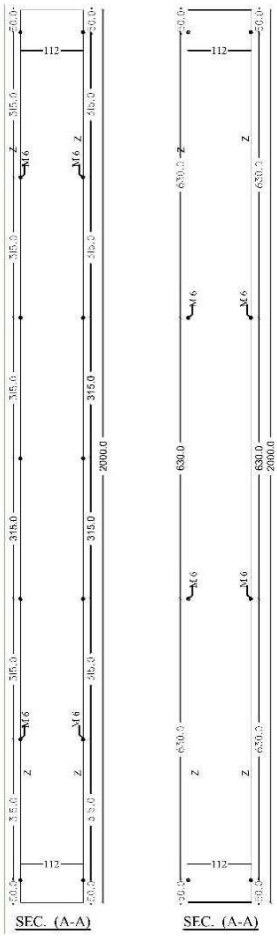

b. Column length(2000mm) with varying spacing 315mm and 630mm between screws

Fig.(6.a, b) Length of column and screw arrangements

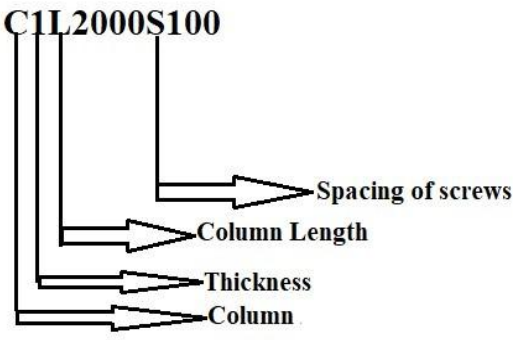

Fig.(7) Label for the specimen

Table (2) Dimensions of parametric study's specimen.

Specimen	Length	Z section				C section				r	S
		H	b_1	c_1	e	h	b_2	c_2	$t_{Z\&C}$		
	(mm)	(mm)	(mm)	(mm)	(mm)	(mm)	(mm)	(mm)	(mm)	(mm)	(mm)
C1L1200S100	1200								1		100
C1L2000S100	2000								1		100
C2L1200S100	1200								2		100
C2L2000S100	2000								2		100
C1L3000S100	3000								1		100
C2L3000S100	3000	250	56.8	22.8	13.44	112	36	20	2	2.8	100
C1L4500S100	4500								1		100
C2L4500S100	4500								2		100
C1L2000S300	2000								1		315
C1L2000S500	2000								1		630

4. Discussion

4.1 Failure modes' shape

Table 3 summarizes the maximum load capacities and failure scenarios for each model. Buckling causes three basic failure modes in columns subjected to axial loads: distortional buckling, flexural buckling, and local buckling.

For Specimen C2L2000S100, at load 351.6 Kn, local buckling waves developed in the middle of the column flanges and the top and bottom of the column web. The amplitude of the local buckling waves extended to the column's web and flanges along its height after the load reached column 475 Kn. Finally, Fig. 8 shows the observation of the Local Buckling (LB) Failure Mode and Distortional Buckling (LDB) at the Ultimate Load of 518.7 Kn.

Local buckling waves, however, began at the top and bottom of the column web for specimen C2L3000S100 at a load of 267.6kN. As the load increased to 298kN, the amplitude of the local buckling waves expanded to the specimen flanges and web. When the load increased to 318.5kN, a slight flexural buckling occurred in the built-up column. Additionally, as Fig. 8 shows, the failure mode at load values of 338 kN showed an interaction between local and flexural-distortional buckling (L- FDB).

Table(3) Numerical ultimate loads and failure modes for columns.

Specimen	PuFE (KN)	Failure Mode
C1L1200S100	188.61	L+D
C2L1200S100	518.63	L+D
C1L2000S100	182.55	L+D
C2L2000S100	508.36	L+D
C1L3000S100	178.37	L+D
C2L3000S100	338.90	L+D
C1L4500S100	151.61	L+F
C2L4500S100	298.23	L+F
C1L2000S315	171.22	L+D+F
C1L2000S630	162.66	L+D+F

As shown in Figure 8, the Zee section buckled in columns between connectors in both the tested column and the FE model. This effect is caused by different connector spacing. Local buckling and distortion buckling are comparable in cold-formed channels.

C1L2000S315 and C1L2000S630 with two half-wave Therefore, distortional or locally warped shapes exist in a single Zed section between Channel.

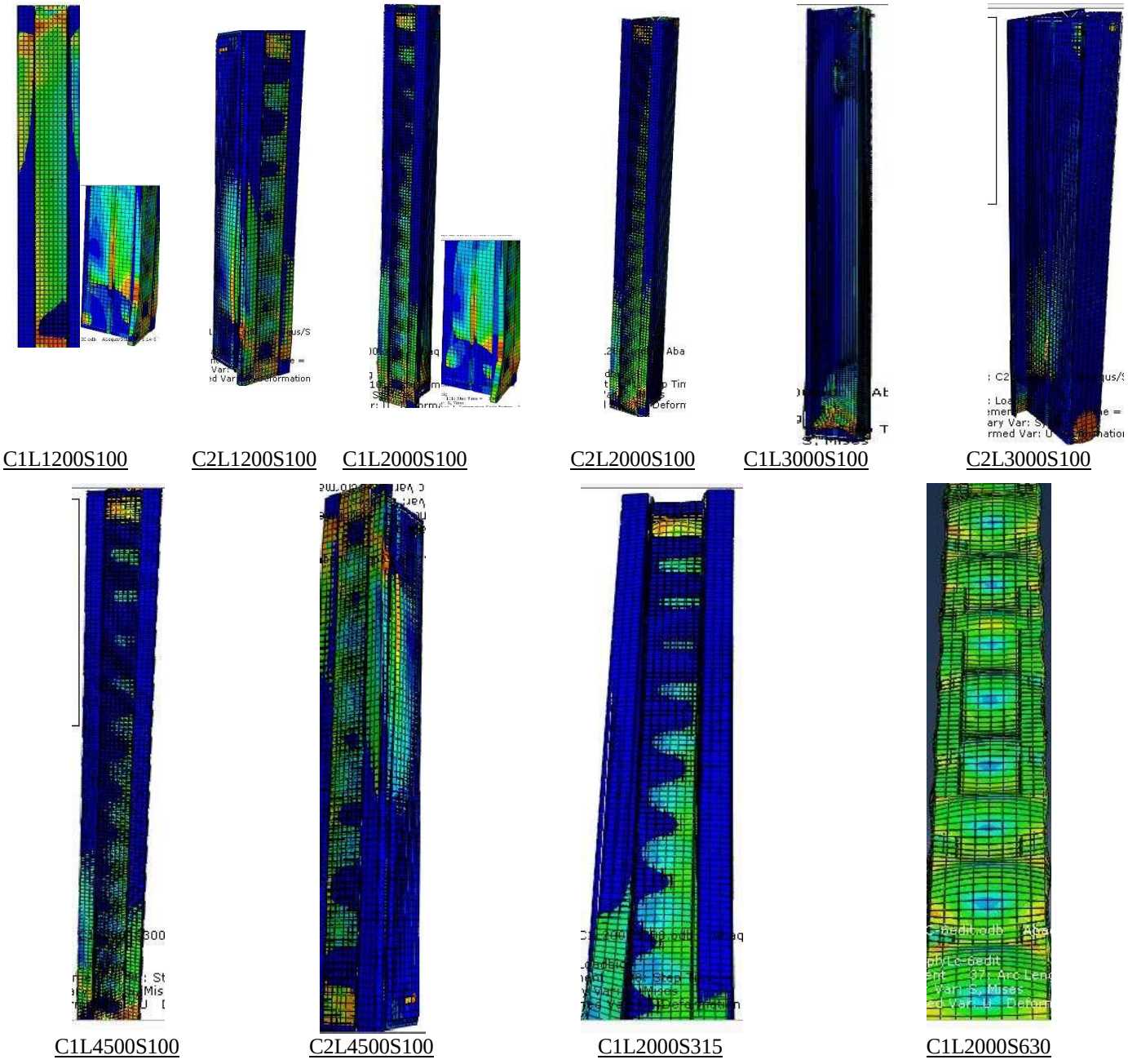

Fig.(8) Failure Mode for columns

4.2 Axial shortening versus axial load

The load against the axial shortening characteristic was linear for nearly all specimens up to 80% of their ultimate load. The nonlinear behavior dominates in the analyzed columns that have entered the post-buckling range, as the end-shortening exceeded the critical buckling load. In the post-buckling range, the graph showed a gradual increase in load alongside a significant rise in end shortening, as seen by a subtle gradient in the curve. The reduction in load was incremental throughout all columns section tested. The behavior remained consistent regardless of the specimens' thickness. The significant ductility was demonstrated by an extended horizontal peak after the attainment of the ultimate load.

Figures 10 show the load-axial shortening curves for various section thicknesses and column lengths for a column with geometries C1L1200S100, C1L2000S100, C2L1200S100, C1L3000S100, C2L3000S100, C1L4500S100, C2L4500S100, and C2L2000S100, respectively.

Figure 11 shows the load versus axial shortening curves obtained from the finite element models, which incorporate contact and variable connector spacing, for the columns with geometries C1L2000S3100,C1L2000S315 and C1L2000S630, respectively.

Column depth-to-width ratio (H/B) for the same cross-section affects axial columns' axial shortening and peak axial strength. As an illustration, columns with a H/B ratio 2.2 showed a decrease in peak axial strengths of 8.6% for the column. It was found that the axially loaded column was stiffer than the columns subjected to other loading types after comparing models with the same column diameter (H/B) but various loading types.

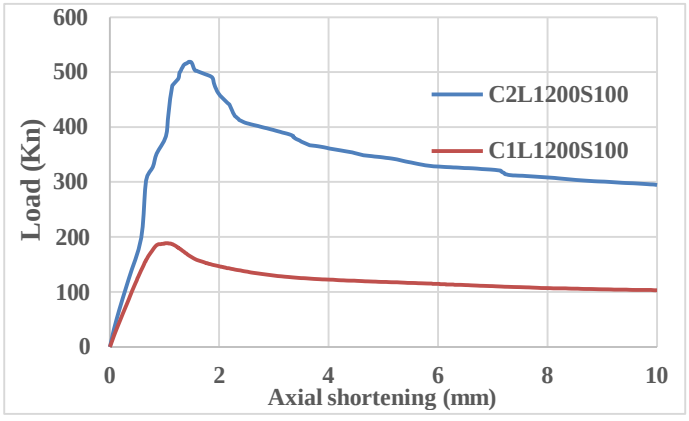

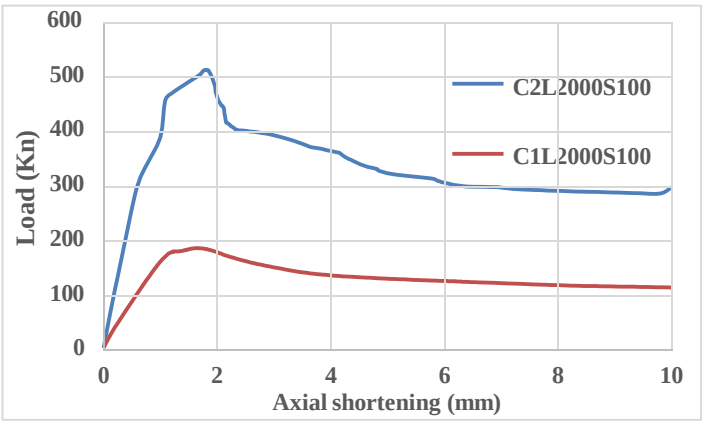

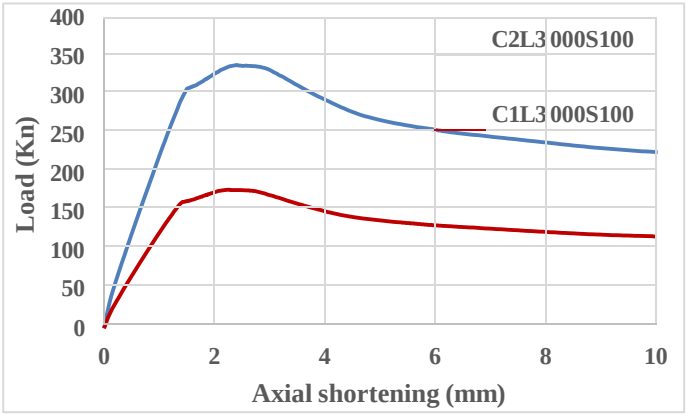

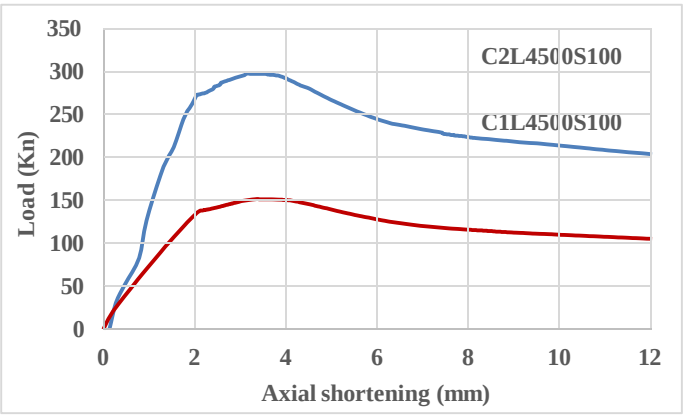

Fig.(10) Relationships between load and axial shortening for colu with varying column thicknesses

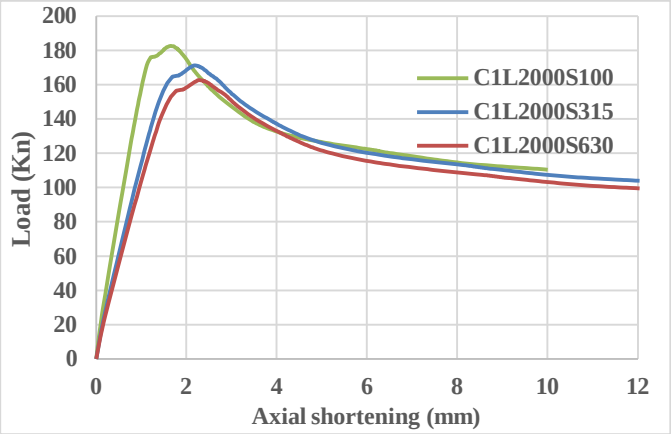

Fig.(11) Relationships between load and axial shortening for columns with varying screw spacing

5. Conclusion

The ultimate capacity of columns composed of identical zee sections with a stiffener in the web and channel utilizing a self-tapping screw configuration was investigated using a nonlinear finite element model. Both geometric and material nonlinearities were taken into consideration in the models. The failure modes for axially loaded columns differed according to the section thickness and length.

Short columns: The main mode of failure was local buckling.

Long columns: Failure was dominated by flexural buckling.

Intermediate columns: Interactive buckling, which combines flexural and local buckling, was the cause of the failure.

Columns with a thickness of 1 mm exhibited greater axial shortening and reduced load capacity. In contrast, columns with a thickness of 2 mm demonstrated less axial shortening and increased load capacity.

The load with axial shortening behavior was linear in almost every specimens to an 80% of its ultimate load. The high degree of ductility was indicated by a long horizontal plateau on reaching the ultimate load.

The lateral deflection behaviour was meager upto ultimate load and thereafter the deflections are predominantly large. The strength drop for column cross-sections with intermediate

References

[1] S. Torabian, D.C. Fratamico, B.W. Schafer, Experimental response of cold-formed steel Zee section beam-columns, Thin-Walled Structures, 98 (2016) 496-517.

[2] AISI S100-12, North American specification for the design of cold-formed steel structural members, 598 American Iron and Steel Institute (AISI), Washington, DC, USA, (2012).

[3] I. Georgieva, L. Schueremans, L. Pyl, L. Vandewalle, Numerical study of built-up double-Z members in bending and compression, Thin-Walled Struct. 60 (2012) 85–97.

[4] S. Gunalan et al. Improved design rules for fixed ended cold-formed steel columns subject to flexural–torsional buckling Thin-Walled Struct. (2013).

[5] S. Gunalan et al. Flexural-torsional buckling behaviour and design of cold-formed steel compression members at elevated temperatures Thin-Walled Struct.(2014)

[6] I. Georgieva, L. Schueremans, L. Vandewalle, L. Pyl, Design of built-up cold-formed steel columns according to the direct strength method, Procedia Eng. 40 (2012) 119–124.

[7] Ferhan Öztürk, Seyed Mohammad Mojtabaei, Mehmet Şentürk, Selim Pul, Iman Hajirasouliha, Buckling behaviour of cold-formed steel sigma and lipped channel beam–column members, Thin- Walled Struct. 173 (2022) 108963.

[8] Qiu-Yun Li, Ben Young, Tests of cold-formed steel built-up open section members under eccentric compressive load, J. Constr. Steel Res. 184 (2021) 106775.

[9] ABAQUS Analysis User's Manual-Version 6.16, ABAQUS Inc., USA, 2016.

[10] S. Nie, T. Zhou, M.R. Eatherton, J. Li, Y. Zhang, "Compressive behavior of built-up double-box columns consisting of four cold-formed steel channels ," Eng. Struct. 222 (2020), 111133.

[11] X. Zhou, Y. Xiang, Y. Shi, L. Xu, Y. Zou, "Simplified design method of cold-formed steel columns with built-up box sections," Eng. Struct. 228 (2021), 111532.

[12] Krishanu Roy, Mohammadjani Chia, B. James, P. Lim, Experimental and numerical investigation into the behaviour of face-to-face built-up cold-formed steel channel sections under compression, Thin-Walled Struct. 134 (2019) 291–309.

.